Mater. Res. Soc. Symp. Proc. Vol. 1538 © 2013 Materials Research Society
DOI: 10.1557/opl.2013.505

Effect of Growth Pressure and Gas-Phase Chemistry on the Optical Quality of InGaN/GaN Multi-Quantum Wells

E.A. Armour[1], D. Byrnes[1], R.A. Arif[1], S.M. Lee[1], E.A. Berkman[1], G.D. Papasouliotis[1], C. Li[2], E.B. Stokes[2,5], R. Hefti[3], and P. Moyer[4,5]

[1] Veeco Instruments, Turbodisc Operations, 394 Elizabeth Avenue, Somerset, NJ 08873, U.S.A.

[2] Department of Electrical and Computer Engineering, University of North Carolina at Charlotte, 9201 University City Blvd, Charlotte, NC 28223, U.S.A.

[3] Nanoscale Science Program, University of North Carolina at Charlotte, 9201 University City Blvd, Charlotte, NC 28223, U.S.A.

[4] Department of Physics & Optical Science, University of North Carolina at Charlotte, 9201 University City Blvd, Charlotte, NC 28223, U.S.A.

[5] Center for Optoelectronics and Optical Communications, University of North Carolina at Charlotte, 9201 University City Blvd, Charlotte, NC 28223, U.S.A.

ABSTRACT

Blue light-emitting diodes (LED's), utilizing InGaN-based multi-quantum well (MQW) active regions deposited by organometallic chemical vapor epitaxy (OMVPE), are one of the fundamental building-blocks for current solid-state lighting applications. Studies [1,2] have previously been conducted to explore the optical and physical properties of the active MQW's over a variety of different OMVPE growth conditions. However, the conclusions of these papers have often been contradictory, possibly due to a limited data set or lack of understanding of the fundamental fluid dynamics and gas-phase chemistry that occurs during the deposition process.

Multi-quantum well structures grown over a range of pressures from typical low-pressure production processes at 200 Torr, up to near-atmospheric growth conditions at 700 Torr, have been investigated in this study. At all growth pressures, clear trends of gas-phase chemical reactions are observed for increased gas residence times (lower gas speeds from the injector flange and lower rotation rates) and increased V/III ratios (higher NH_3 flows).

Confocal microscopy, excitation-dependent PL (PLE), and time-resolved photo-luminescence (TRPL) have been employed on these MQW structures to investigate the carrier lifetime characteristics. Confocal emission images show spatially-separated bright and dark regions. The bright regions are red-shifted in wavelength relative to the dark regions, suggesting microscopic spatial localization of high indium content regions. As the growth pressure and gas residence times are reduced, a larger difference in band-gap between bright and dark regions, longer lifetimes, and higher average PL intensities can be obtained, indicating that higher optical quality material can be realized. Optimized MQW's grown at high pressure exhibit higher PLE slope intensities and IQE characteristics than lower pressure samples. Results on simple LED structures indicate that the improvement in MQW optical quality at high pressures translates to higher output power at a 110 A/cm^2 injection current density.

INTRODUCTION

As InGaN-based LED epi-structure brightness and electrical performance continues to be improved, primarily through structural and process recipe optimization, there exists a desire to more completely understand the fundamental material and gas-phase chemistry limitations influencing these parameters. Current production-level LED structures are typically grown at low-pressure conditions for the MQW active region (≤ 200 Torr), where the reactor designs can maintain extremely reproducible and uniform performance. However, there have been limited reports on the chemical mechanisms that occur during the InGaN OMVPE process [1,3-6] and the process optimization needed to achieve high quality material. Of particular interest is the effect that growth pressure has on the optical and morphological properties of the InGaN material.

To understand these properties over a wide range of process conditions, we have employed a simple 4-period thin InGaN MQW structure. The growths were performed in a Veeco K465i Turbodisc reactor, utilizing vertical geometry and high-speed rotation. All growths were performed with equivalent plug-flow stability parameters, whereby the total flow into the reactor matched the rotationally-driven pumping speed of the disk to achieve laminar and stable fluid flow streamlines. More details of a high speed rotating disk reactor operation can be found in [7].

EXPERIMENTAL

The MQW samples in this study were grown on planar c-plane oriented (0001) sapphire substrates, miscut 0.2° towards the m-plane. The underlying GaN buffer layers consisted of a 2.2 µm nominally undoped GaN buffer, followed by a 2 µm n-type GaN layer with approximately $7x10^{18}$ cm^{-3} silicon doping level, as measured by SIMS. The XRD FWHM of the GaN templates were controlled to a range of 250-270" for (002)ω and 260-280" for (102)ω rocking curves, which translates into a threading dislocation density of approximately $4.4x10^{8}$ cm^{-2} [8]. The surface morphology of the n-GaN templates was measured using AFM with a 5 x 5 µm scan area, exhibiting a typical roughness of 0.4 nm RMS. Following the n-GaN buffer layers, the MQW structure was deposited, which consisted of 4 pairs of a 2.7 nm InGaN quantum well (QW) sandwiched between 10 nm GaN quantum barriers (QB). Triethylgallium (TEGa) and trimethylindium (TMIn) with nitrogen (N_2) as a carrier gas were used for the QW's. The period growth rate was controlled at 0.9 nm/min. by changing the overall TEGa and TMIn fluxes, keeping a fixed molar ratio of 1.7 to obtain identical structures between the different growth conditions. The same TEGa flow rate was used for both QW and QB layers. Ammonia (NH_3) was used as the group V source. The deposition temperature was controlled using a fixed emissivity pyrometer measuring the wafer carrier, and was adjusted for each growth sample to achieve approximately 450 nm peak PL wavelength.

Our experimental dataset explored the morphological and optical quality of the MQW's as a function of growth pressure, V/III ratio, and total flow of the gases. The total flow is determined by the amount of N_2 carrier gas and NH_3 injected into the reactor. In these experiments, relatively small changes in NH_3 flows were used (in a range of 30 to 70 slm), such that the N_2 carrier gas flow usually dominated the total flow ratio. Low-power photoluminescence (PL) maps were acquired and averaged over two 4" diameter full wafer samples, using a Nanometrics RPM Blue with a pump wavelength of 377 nm and an incident power of ~127 W/cm^2.

To more accurately assess the optical quality of the films closer to the carrier densities employed in typical LED structures, power-dependent PL excitation (PLE) spectroscopy was utilized. For our PLE experiments, the center point of the 4" wafer was pumped with a frequency doubled Ti:sapphire femtosecond laser operating at 76 MHz with an illumination wavelength of 375 nm. The output of the second harmonic generator was coupled to a fiber and focused on the sample with a spot size of approximately 1 mm diameter. The PLE measurements were conducted over an average incident power in the range of 6 mW to 160 mW, which corresponds to an estimated injection current density of 6 to 150 A/cm^2. The integrated intensity as a function of illumination power was plotted, and the slope of this curve was used as a metric of "brightness" of each MQW sample.

Confocal laser scanning microscopy (CLSM) was also employed to characterize these samples. A 405 nm pulsed laser beam, with 10 MHz frequency and 300 ps pulse width, was used as an excitation source for the CLSM measurements. The laser was coupled into a single mode optical fiber after which a 405/20 nm band pass filter (BPF) was placed to block any fluorescence emission from the fiber. The laser beam was then reflected by a 430 nm dichroic beam splitter (DBS) to a 100× objective lens whose numerical aperture is 1.25. The objective lens focused the laser beam onto the samples, and also collected PL emitted from the samples. PL collected by the objective lens passed through the DBS and a pinhole, and then was detected using a time-correlated single photon counting (TCSPC) avalanche photodiode (APD), which was preceded by a 445/40 nm BPF so that only near-band-edge emission light contributed to the imaging. The optical probe was stationary relative to the instrument frame, while the sample was mounted to a high speed scanning lead zirconium titanate (PZT) stage with nanometer precision control along three axes and a translation range of 70 μm by 70 μm by 50 μm in x-, y-, and z-directions, respectively. The microscope had a lateral spatial resolution of about 200 nm, and vertical spatial resolution of about 100 nm. Localizing features to better than 5 nm is possible using deconvolution with a point spread function. With suitable synchronization and time-counting software, the system could also be used to measure time-resolved PL (TRPL) of micrometer or nanometer scale structures. For spectral measurements, the 445/40 nm BPF and TCSPC APD were replaced by a spectrometer equipped with a thermoelectrically-cooled CCD camera.

RESULTS AND DISCUSSION

At 200 and 450 Torr growth pressures, higher total flows and V/III ratios for a given chamber pressure generally resulted in stronger PL intensities. As the growth pressure was raised, the PL intensity ratio between low flow and high flow conditions increased, with low total flow conditions at 700 Torr having very weak PL signals. For the 700 Torr samples, there was also a substantial improvement in surface morphology as the total flow was increased, as illustrated in Figure 1. With low total flows (i.e. long gas residence time in the chamber), samples under these conditions exhibited 3-dimensional indium inclusions and a Stranski-Krastanov type of growth mode. As the total flow increases, we observed a transition through a spiral growth mode pattern towards a two-dimensional step-structure morphology.

At 700 Torr pressure, increasing the V/III ratio did not result in improved PL intensity, but instead reduced the intensity, unlike the cases for 200 Torr and 450 Torr. To achieve equivalent

PL intensities between 50 slm NH_3 and 70 slm NH_3 flows, the total flow for these conditions needed to be increased by approximately 20%

.

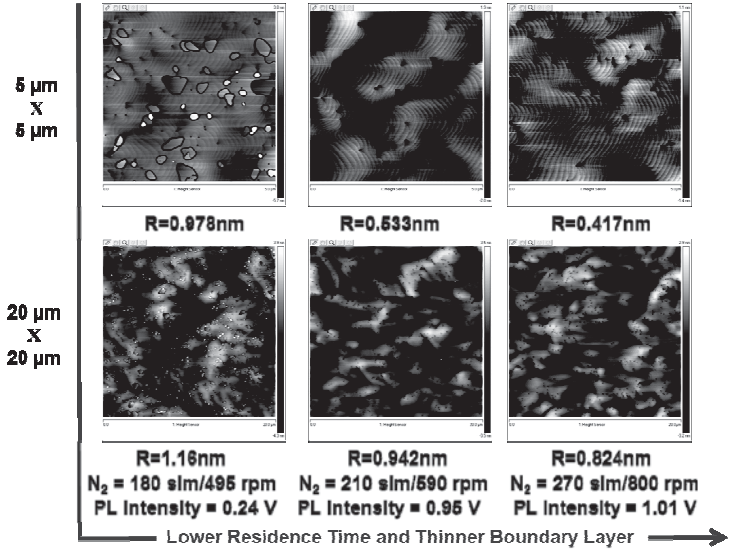

Figure 1. Surface morphology for 700 Torr MQW's as a function of N_2 carrier flow with NH_3 flow at 50 slm.

These characteristics reinforce the observations that we previously published [9], suggesting that parasitic gas-phase reactions occur between TEGa, TMIn, and NH_3, and are particularly amplified at higher process pressure. The gas-phase reactions are likely changing the ratio of chemical adducts adsorbing onto the growth surface, which affect the adatom surface diffusion characteristics. This explanation endorses the proposal of [1], which suggested that as pressure is increased, the adatom surface diffusion may be impeded by either adsorbed reactants or carrier gas species. However, from our total flow experiments where only the N_2 carrier gas is being modulated, it does not appear that adsorbed carrier gas species (N_2) are necessarily suppressing adatom surface diffusion.

Two effects occur when total flow is increased: (a) residence time of the chemical species is reduced between injection at the top flange down to the thermal and momentum boundary layers, which is proportional to the gas speed, and (b) the boundary layer is compressed due to increased rotation required to balance the higher total flow. It should be pointed out, however, that continually increasing the N_2 flow rate to achieve even larger total flows results in a reduced partial pressure of the NH_3 species, which is not desirable do to its negative effect on MQW (InGaN) quality.

To more easily understand the optimized process parameter space, we have developed two metrics to describe the gas residence time to the growth surface and the effective amount of NH_3 that is available for growth:

S* = (gas velocity at injector plate) x (wafer carrier rotation speed)

$$V/III^* = \frac{\#\text{ of moles of } NH_3 * X_{NH3}}{\#\text{ of moles of Alkyls}}$$

with

$$X_{NH3} = \frac{NH_3\ flow}{NH_3\ flow + N_2\ flow}$$

where S* is defined as the effective gas speed, and V/III* is the diluted V/III ratio, which is influenced by the NH_3 partial pressure ratio. Using these two parameters, for a fixed QW growth rate and TEGa/TMIn molar ratio, we can easily compare optical qualities from one condition to another in a normalized process space.

As can be seen from the 200 Torr and 450 Torr contour plots of Figure 2, as the effective gas speed S* is increased simultaneously with V/III* (diagonal upwards indicated by the arrows), the PL intensity increases for the samples. The highest intensities achieved at both pressures occur at a gas speed S* > 90. For 700 Torr conditions, very high brightness samples can be obtained, although the increased S* vs. V/III* trend observed at the lower pressures is obfuscated. At this high growth pressures, the process space becomes more limited due to the smaller achievable gas velocities and higher total flows (i.e. N_2 carrier gas flow) necessary to achieve stable plug flow. At 700 Torr, laminar streamlines without recirculation cells are hard to obtain due to geometrical limitations in the injector design, which limits the run-to-run repeatability needed to fully characterize this process space.

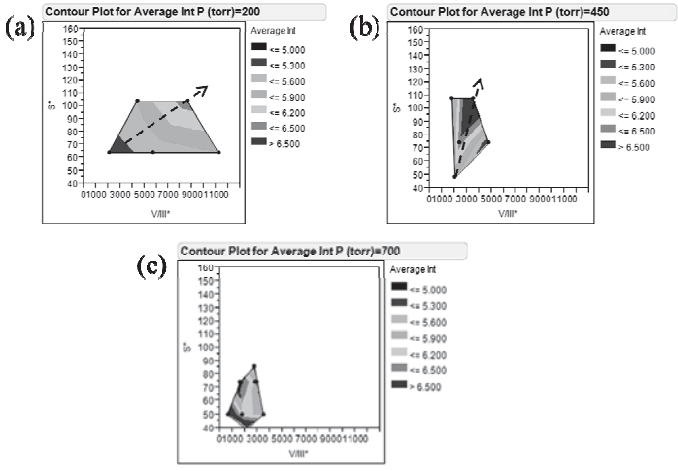

Figure 2. PL Intensity as a function of effective Gas Speed (S*) and effective V/III ratio (V/III*) for (a) 200 Torr, (b) 450 Torr, and (c) 700 Torr growth pressures.

Another observation is that when pressure is increased, a higher wafer carrier temperature is needed to achieve similar indium concentrations in the MQW and hence maintain the target wavelength of 450 nm. Typically, about 5-8° C increase is necessary between similar 200 Torr and 450 Torr conditions, and another 8-12° C increase is needed to achieve the same wavelength at 700 Torr conditions. Measurements using an in-situ 405 nm pyrometer (Veeco BluTemp^{TM}) indicate that for these controlled structures, the surface temperature remains the same, and that the differential temperature between the wafer carrier and wafer enlarges with increasing temperature [10]. It is proposed that convective surface cooling at the wafer relative to the wafer carrier from the higher density of gas and higher total flows at the higher pressures may be the driving forces for this difference. The higher gas temperature in the vicinity of the wafer carrier could also result in increased pyrolysis of the NH_3, resulting in a higher effective V/III ratio at the growth surface for the high pressure conditions.

Table I. Summary of PLE, CLSM, and TRPL measurements for a subset of the explored growth conditions.

Sample ID	Growth pressure (torr)	V/III*	S*	PLE slope Efficiency	CLSM Images average intensity	Bandgap difference (meV)	PL peak intensity ratio	PL lifetime τ2 in bright region (ns)	PL lifetime τ2 in dark region (ns)
1	200	4457	104	44.84	70	44.2	3.63	22.94	18.97
2	200	2123	64	35.41	49	39.1	3.25	17.99	15.17
3	200	5778	64	34.32	54	25.4	3.01	20.11	16.77
4	200	3820	151	38.80	55	30.5	3.19	17.25	16.75
5	200	4504	104	36.60	60	37.5	3.34	21.41	18.88
6	200	3016	104	48.59	66	41.6	3.55	25.31	20
7	450	2463	74	35.44	60	35.3	3.27	17.86	14.82
8	450	1851	108	68.93	80	41.5	3.58	27.75	22.31
9	450	2092	48	30.78	44	22.8	2.93	15.72	11.31
10	450	8948	74	56.50	64	47.9	3.79	23.87	19.34
11	700	3572	50	50.84	71	36.9	3.3	26.85	24.17
12	700	684	50	42.70	52	27.1	3.09	23.85	22.57
13	700	2979	75	65.11	88	45.3	3.61	27.44	24.34
14	700	3668	81	39.84	57	27.6	3.11	23.67	22.63

Combined results of PLE, CLSM, and TRPL measurements for MQW's grown over a selection of different flow conditions are listed in Table I. PLE slope is determined by integrating the intensity over the pump laser power, and is suggested to be the best metric for translating to LED optical power efficiency, due to the high carrier injection intensities that are generated. The CLSM image average intensity was calculated by averaging the intensity of each pixel of the image obtained during the measurements. There is a rough correlation of PLE intensity to CLSM intensity, as indicated in Figure 3 (a). Figure 3 (b) shows the PLE slope efficiency as a function of effective gas speed S* plotted with identification of different pressures. In both measurement cases, the strongest PL intensity samples are obtained at higher

pressure (450 Torr and 700 Torr) growth conditions. Similar levels of PL intensity could not be achieved at 200 Torr growth conditions, even after process optimization.

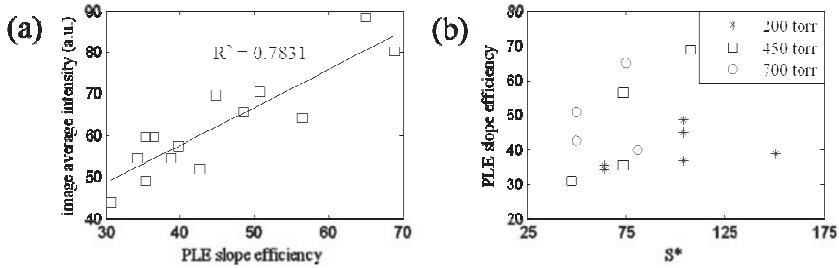

Figure 3. a) Correlation of PLE slope efficiency to CLSM image average intensity, (b) PLE slope efficiency as a function of effective gas speed (S*) for different growth pressures. Note the highest intensity samples are at 450 Torr and 700 Torr.

Figure 4 shows the CLSM image of near band-edge emission for a MQW sample grown at 700 Torr, in which an inhomogeneous distribution of PL intensity is observed. Bright regions, which are several micrometers in size, are surrounded by considerably dimmer dark regions. PL spectra measured at different places in the image show that the intensity at bright regions is > 3 times stronger than that in the dark regions, as indicated by the peak ratio in Table I. Furthermore, the PL peaks in the bright regions are red-shifted compared with the PL peak in the dark regions, as is shown in Figure 5 (a). This is consistent with smaller band-gap energy in the bright regions more effectually localizing carriers to recombine radiatively, and thus preventing them from migrating to regions with non-radiative recombination defect centers (NRRCs). The darker regions, on the other hand, exhibit higher band-gap energies and reduced potential well height, thus more easily allowing thermal diffusion into the NRRC sections. The average image PL intensity increases when the band-gap energy difference between these regions becomes larger, as shown in Figure 6 (a). As the CLSM image average intensity increases, the image becomes less uniform, as the image standard deviation, which is defined as how much variation or exists from the average, is larger for samples with larger image average intensity. This is shown in Figure 6 (b) and is to be expected, as samples with higher average intensity have a larger band-gap energy difference and stronger carrier localization effect in its narrow-band-gap-region, resulting in a larger difference between bright and dark region PL intensities.

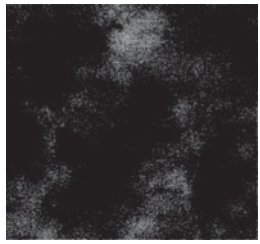

Figure 4. Confocal microscope image of 445 nm near band-edge emission for a 700 Torr MQW sample. The image uses a 40 nm band-pass filter, illustrating the bright and dark regions. The image covers a 20 μm × 20 μm region in the center of the sample wafer.

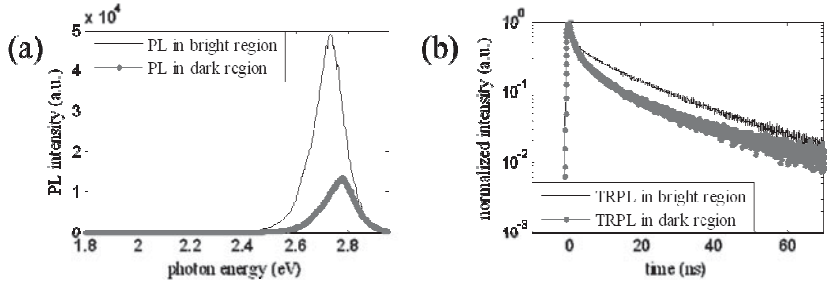

Figure 5. (a) Confocal PL spectra at bright and dark regions on the image in Figure 4, and (b) TRPL lifetime decay plots of the bright and dark regions.

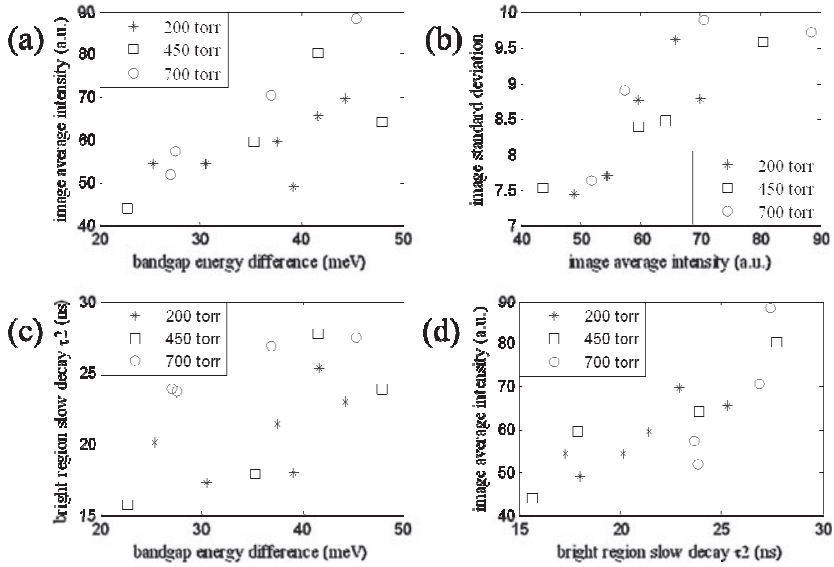

Figure 6. (a) CLSM image average intensity as a function of band-gap energy difference between bright and dark regions of the MQW samples from this study, (b) CLSM image average intensity compared to the contrast between bright and dark regions, (c) CLSM image average intensity as a function of τ2 lifetime of the bright regions in the sample, and (d) τ2 lifetime plotted against band-gap energy difference for the sample MQW's.

Confocal TRPL measurements were performed in both bright and dark regions on each sample. Figure 5 (b) shows the TRPL spectra for the sample that was pictured in Figure 4. A bi-exponential decay equation was used to fit the TRPL spectra, and two lifetimes τ1 and τ2 were obtained, where τ1 is a fast observed decay component (no more than 3 ns) and τ2 is a slower observed decay component (around 20 ns). The biexponential function is consistent with two spatially distinct recombination systems in each probed region. In our analysis, τ2 is attributed to recombination in the strongly localized states, while τ1 is attributed to weakly localized states where radiative recombination is more quenched by NRRC and also competes with carrier transfer into strongly localized states. As a result, the slow decay lifetime τ2 tends to dictate the overall optical quality of the MQW samples, as plotted in Figure 6 (b). The lifetime of τ2 within the bright regions is longer than the τ2 within the dark regions, indicating higher quenching of recombination in strongly localized states in dark regions. The shorter lifetime and lower intensity of dark regions is consistent with a higher level of recombination through NRRC in the dark regions, and/or carrier transport from dark-to-bright regions. The longer τ2 lifetime in bright regions also coincides with a larger band-gap energy difference between the bright and dark regions, which is consistent with our explanations above, as evidenced in Figure 6 (c).

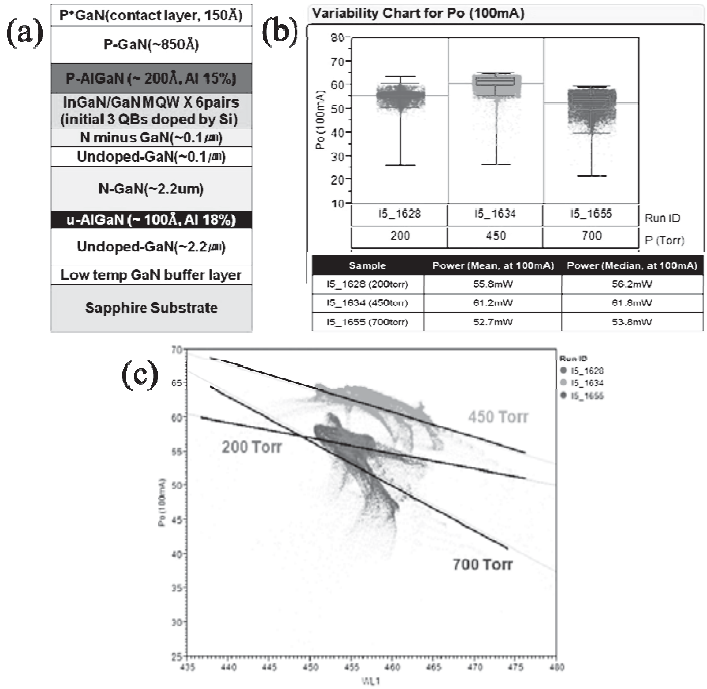

Figure 7. (a) LED epitaxial structure, (b) light output power (LOP) histogram measured for the 3 different pressures using optimized MQW flow conditions, and (c) output power plotted as a function of wavelength (nm) for the 3 LED wafers.

The flow conditions yielding the highest PLE slope efficiency for each pressure were selected to insert into the 6-pair MQW active region of a simple LED structure, which is shown in Figure 7 (a). For all 3 LED's tested, the same structure and doping levels were used, and only the active layer growth conditions were changed. The fabricated LED die were 300 μm x 300 μm in size, with a lateral electrode configuration, mesa-etched and passivated, but not separated. A production prober was used to map die throughout the entire wafer; no special temperature control was used during the measurements.

The LED devices with MQW's grown at 450 Torr were brighter than 200 Torr MQW LED's by ~ 9.7%, whereas the 700 Torr LED's were slightly dimmer, as shown in the histogram of Figure 7 (b), and the output power as a function of wavelength plots of Figure 7 (c). The brightness increase between 200 Torr and 450 Torr MQW optimized growth conditions has been confirmed through repeated growth and fabrication LED campaigns, averaging a 5-10% improvement in optical output power. Reference wafers during each fabrication campaign yielded batch-to-batch variations of < 5%. The drop in power for the 700 Torr LED was not entirely unexpected, as the 450 Torr conditions are within the plug-flow stability regime, but the 700 Torr MQW flow conditions have non-laminar streamlines, which can lead to large run-to-run variations. It should be noted that optimized higher pressure growths have also shown improvements in optical power output in customer structures and other LED studies [11].

CONCLUSIONS

Multi-quantum well structures have been studied over a variety of growth conditions to examine the morphology and optical quality of the materials grown. At increased growth pressures, parasitic chemical reactions can dominate, reducing material quality. To lessen the effect of these chemical pathways, decreasing gas residence time by increasing total flow can improve overall PL intensity. To further understand the relationship between growth conditions and PL intensity, we have developed two metrics: effective gas speed S* and diluted V/III* which allow us to compare growth conditions over a wide process space. For long gas residence time (low S*) and high V/III* conditions, gas-phase chemical reactions are amplified, resulting in a reduced parameter space to achieve high-quality MQW layers. This trend is particularly clear at high MQW growth pressures, where suppressing gas phase reactions with high total flows for high V/III ratio material results in higher PL intensity structures. Under optimized conditions, our brightest samples were achieved at elevated growth pressures.

Optical characterization of the MQW samples using power-dependent PL excitation, confocal laser scanning microscopy, and time resolved PL have shown that the highest emission samples have stronger localization with a greater difference in band-gap between bright and dark regions, and exhibit longer TRPL lifetimes. Initial LED studies incorporating equivalent MQW structures and optimized flow conditions have exhibited higher optical output power for 450 Torr samples when compared to 200 Torr samples.

ACKNOWLEDGEMENTS

The authors wish to acknowledge Frank Lu for assistance on TRPL and PLE optical measurements and Steve Ting for helpful suggestions.

REFERENCES

1. R.A. Oliver, M. J. Kappers, C.J. Humphreys, and G.A.D. Briggs, J. Appl. Phys. **97**, 013707 (2005).
2. W.V. Lundin, E.E. Zavarin, M.A. Sinitsyn, A.V. Sakharov, S.O. Usov, A.E. Nikolaev, D.V. Davydov, N.A. Cherkashin, and A.F. Tsatsulnikov, Fiz. Tekh. Poluprovodnikov **44**, 126, (2010) [Semiconductors **44**, 123 (2010)].
3. J.R. Creighton, G.T. Wang, W.G. Breiland, and M.E. Coltrin, J. Crystal Growth **261**, 204 (2004).
4. J.R. Creighton, M.E. Coltrin, and J.J. Figiel, Appl. Phys. Lett. **93**, 171906 (2008).
5. G.B. Stringfellow, J. Crystal Growth **312**, 735 (2010).
6. A, Demchuk, J. Porter, and B. Koplitz, J. Phys. Chem. A **102**, 8841 (1998).
7. B. Mitrovic, A. Gurary, and L. Kadinski, J. Crystal Growth **287**, 656 (2006).
8. S.R. Lee, A.M. West, A.A. Allerman, K.E. Waldrip, D.M. Follstaedt, P.P. Provencio, D.D. Koleske, and C.R. Abernathy, Appl. Phys. Lett. **86**, 241904 (2005).
9. E.A. Armour, B. Mitrovic, A. Zhang, C. Ebert, M. Pophristic, and A. Paranjpe in *Compound Semiconductors for Generating, Emitting and Manipulating Energy*, edited by T. Li, M. Mastro, A. Dadgar, H. Jiang, and J. Kim, (Mater. Res. Soc. Symp. Proc. **1396**, Boston, MA, 2011) pp. 3-14.
10. Alexander Manasson, private internal Veeco communication (2013).
11. J.H. Na, S.K. Lee, H.S. Lim, H.K. Kwon, S. Son, and M.S. Oh, presented at the 16th International Conference on Metal Organic Vapor Phase Epitaxy, Busan, Korea, 2012 (unpublished).